



Missouri University of Science and Technology  
Scholars' Mine

Geosciences and Geological and Petroleum  
Engineering Faculty Research & Creative Works

Geosciences and Geological and Petroleum  
Engineering

01 Feb 2015

## A Systematic Comparison of the Transverse Energy Minimization and Splitting Intensity Techniques for Measuring Shear-Wave Splitting Parameters

Fansheng Kong

Stephen S. Gao

Missouri University of Science and Technology, [sgao@mst.edu](mailto:sgao@mst.edu)

Kelly H. Liu

Missouri University of Science and Technology, [liukh@mst.edu](mailto:liukh@mst.edu)

Follow this and additional works at: [https://scholarsmine.mst.edu/geosci\\_geo\\_peteng\\_facwork](https://scholarsmine.mst.edu/geosci_geo_peteng_facwork)



Part of the [Geology Commons](#), and the [Numerical Analysis and Scientific Computing Commons](#)

### Recommended Citation


F. Kong et al., "A Systematic Comparison of the Transverse Energy Minimization and Splitting Intensity Techniques for Measuring Shear-Wave Splitting Parameters," *Bulletin of the Seismological Society of America*, vol. 105, no. 1, pp. 230-239, Seismological Society of America, Feb 2015.

The definitive version is available at <https://doi.org/10.1785/0120140108>

This Article - Journal is brought to you for free and open access by Scholars' Mine. It has been accepted for inclusion in Geosciences and Geological and Petroleum Engineering Faculty Research & Creative Works by an authorized administrator of Scholars' Mine. This work is protected by U. S. Copyright Law. Unauthorized use including reproduction for redistribution requires the permission of the copyright holder. For more information, please contact [scholarsmine@mst.edu](mailto:scholarsmine@mst.edu).

# A Systematic Comparison of the Transverse Energy Minimization and Splitting Intensity Techniques for Measuring Shear-Wave Splitting Parameters

by Fansheng Kong, Stephen S. Gao, and Kelly H. Liu

**Abstract** Over the past several decades, shear-wave splitting (SWS) analyses have been increasingly utilized to delineate mantle structure and probe mantle dynamics. However, the reported splitting parameters (fast polarization orientations and splitting times) are frequently inconsistent among different studies, partially due to the different techniques used to estimate the splitting parameters. Here, we report results from a systematic comparison of the transverse minimization (TM) and the splitting intensity (SI) techniques. The study was motivated by the fact that recent comparative studies led to conflicting conclusions, which include the suggestion that TM, which is arguably the most widely used SWS-measuring technique, performs significantly poorly relative to SI under most circumstances in terms of stability and reliability of the resulting splitting parameters. We use both synthetic and real seismograms to evaluate the performance of the techniques for noise resistance, dominant period dependence, and complex anisotropy recognition. For one-layer anisotropy models with a horizontal axis of symmetry, our results show the two techniques can provide measurements with similar reliability. The testing confirms conclusions from previous studies that, although SI cannot distinguish between simple and complex anisotropy models with a horizontal axis of symmetry, TM can serve as a powerful tool in recognizing the existence of complex anisotropy, which is characterized by a systematic dependence of the splitting parameters on the back azimuth of the events. Therefore, when the existence of complex anisotropy beneath a study area is unknown, TM is a better choice.  A FORTRAN program for the calculation of Wiener-filtered wavelet and splitting intensity using SI technique is provided as an electronic supplement to this article.

*Online Material:* FORTRAN code to calculate splitting intensity.

## Introduction

As demonstrated by numerous previous studies, shear-wave splitting (SWS) analyses using *P*-to-*S* converted phases at the core–mantle boundary (including *PKS*, *SKKS*, and *SKS*; collectively called *XKS*) have been widely utilized as a powerful tool for detecting and characterizing deformational processes in the Earth’s mantle (Bowman and Ando, 1987; Silver and Chan, 1991; Gao *et al.*, 1994, 2010; Savage, 1999; Long and Silver, 2009; Liu *et al.*, 2014). However, the resulting SWS parameters, the fast polarization orientation ( $\phi$ ), and the splitting time ( $\delta t$ ) are frequently dependent on the measuring methodologies (Vecsey *et al.*, 2008). Significant discrepancies exist in published papers conducted by different groups, which led to heated debates concerning the reliability of the resulting splitting parameters and, consequently, their geodynamic implications (e.g., Liu *et al.*, 2008).

Arguably, the most popularly used SWS measuring method is the transverse minimization (TM) method proposed by Silver and Chan (1991). It estimates splitting parameters based on a grid-search technique for the optimal fast orientation and splitting time that can best remove energy on the corrected transverse component. TM is an event-specific measuring technique; that is, each event with a sufficient signal-to-noise ratio (SNR) on both the radial and transverse components will lead to an optimal pair of parameters. For simple anisotropy (i.e., anisotropy characterized by a single layer with a horizontal axis of symmetry), the observed splitting parameters are independent of the back azimuth (BAZ) of the events. For events with a BAZ that is orthogonal or parallel to the fast orientation, or for stations below which the Earth’s crust and mantle is isotropic, no energy on the transverse component will be observed, resulting in a null (N)

measurement (Silver and Chan, 1991). When the anisotropy is complex (i.e., anisotropy that can not be adequately characterized by simple anisotropy), the observed splitting parameters are dependent on the BAZ and thus are not true but apparent parameters. Apparent splitting parameters are frequently used to characterize complex anisotropic structures, for example, multiple layers based on periodicity of splitting parameters over BAZ (e.g., Silver and Savage, 1994; Yang *et al.*, 2014), spatial variation based on ray-piercing point (e.g., Liu and Gao, 2013), and lower mantle contributed splitting based on ray paths of SKS and SKKS (e.g., Niu and Perez, 2004).

The splitting intensity (SI) method was proposed by Chevrot (2000) and has been utilized by several studies for measuring SWS parameters and for tomographic inversion (e.g., Chevrot and van der Hilst, 2003; Monteiller and Chevrot, 2010, 2011; Romanowicz and Yuan, 2012). The splitting intensity for an event is measured by projecting the transverse energy on the derivative of the radial component (Monteiller and Chevrot, 2010). The splitting parameters can be retrieved by fitting the azimuthal variation of the splitting intensities using a sine function, in which the phase shift is related to the fast orientation and the amplitude is proportional to the splitting time (Chevrot, 2000).

Long and van der Hilst (2006) conducted comparative studies of TM and SI using data from two stations in Japan. The splitting parameters observed at station TKA using TM and SI agree well. In contrast, at station SGN, large discrepancies exist between the results obtained using different techniques. Such discrepancies are considered to be the results of complex anisotropy (Long and van der Hilst, 2006). They test the stability of results from different measuring techniques in terms of the frequencies for band-pass filtering and conclude that SI is more robust and stable. Monteiller and Chevrot (2010) test the noise resistance and frequency dependence of resulting splitting parameters obtained by SI and TM using both synthetic and real seismograms recorded by four broadband stations. They apply a Wiener filter to normalize the XKS arrivals from different events to enhance the effective signal on the radial and transverse components. The conclusion from the comparative study is that TM can provide reliable measurements only under ideal circumstances, including large splitting time (e.g.,  $\geq 1.3$  s), short dominant period (e.g.,  $\leq 6.0$  s), and very strong signal on the transverse component, which is possible only when the difference between the BAZ and the fast orientation is close to  $45^\circ$ . For instance, when synthetic data with a low SNR of 3 and a large dominant period of 12 s are used, the SWS parameters calculated using TM are essentially unconstrained. Such a poor performance of TM is also suggested when it is applied to measure the splitting parameters at the four stations (Monteiller and Chevrot, 2010).

This study systematically evaluates the TM and SI techniques in terms of noise resistance, dominant period dependence, and complex anisotropy recognition using both synthetic and real data. In contrast to previous studies, we conclude that for simple anisotropy, SI and TM are similar

in terms of reliability in the resulting splitting parameters, but TM is advantageous in detecting complex anisotropy.

## Testing Using Synthetic Data

### Data Generation

To produce synthetic SKS seismograms under a model of simple anisotropy with a given pair of  $\phi$  and  $\delta t$ , we first define a presplitting radial component in the form of

$$R(t) = A_0 \sin(2\pi ft) e^{-\alpha t}, \quad (1)$$

in which  $A_0 = 1.0$  is the amplitude,  $f$  is the frequency, and  $\alpha = 0.1$  is the decay factor. We then generate 36 synthetic events with a randomly selected BAZ ranging from  $0^\circ$  to  $360^\circ$ . The fast ( $S_f$ ) and slow ( $S_s$ ) components for an event can be computed using

$$S_f(t) = R(t) \cos(\theta) \quad (2)$$

and

$$S_s(t) = -R(t - \delta t) \sin(\theta), \quad (3)$$

in which  $\theta$  is the angle between the fast and radial directions. The resulting fast and slow components are rotated based on the BAZ to create the north–south and east–west components.

To resemble real data that contain noise of various levels, we add noise recorded by station USIN located in Indiana (United States) to the north–south and east–west components. To accomplish this task, about 1500 seismograms recorded by the station are extracted; and, for each seismogram, a 40-s-long noise trace  $N(t)$  is selected in the time window of  $(a - 40, a)$  s, in which  $a$  is the beginning of the SKS window and is 5 s before the IASP91 theoretical SKS arrival time. The noise trace is then detrended and normalized by the mean of the absolute values; that is,

$$N_0(t) = N(t) / \overline{|N(t)|}. \quad (4)$$

A noisy synthetic seismogram with an SNR of  $r$ , defined as  $\max |A_{(a,f)}| / \max |A_{(a-10,a)}|$ , in which  $\max |A_{(a,f)}|$  is the maximum absolute value between  $a$  and  $f$  (the beginning and end of the XKS window) and  $\max |A_{(a-10,a)}|$  is that between  $a - 10$  and  $a$ , is then created using  $r \times C(t) + N_0(t)$ .  $C(t)$  is the noise-free north–south or east–west component, and  $N_0(t)$  is a randomly selected normalized noise trace. Finally, the north–south and east–west traces are rotated to radial and transverse components for splitting analysis. Examples of radial and transverse waveforms with an SNR of 8.0 are shown in Figure 1.

For a two-layer model of anisotropy, the fast and slow components after passing through the lower layer are generated using equations (2) and (3) and are consequently used as waves incident to the upper layer to compute the final fast

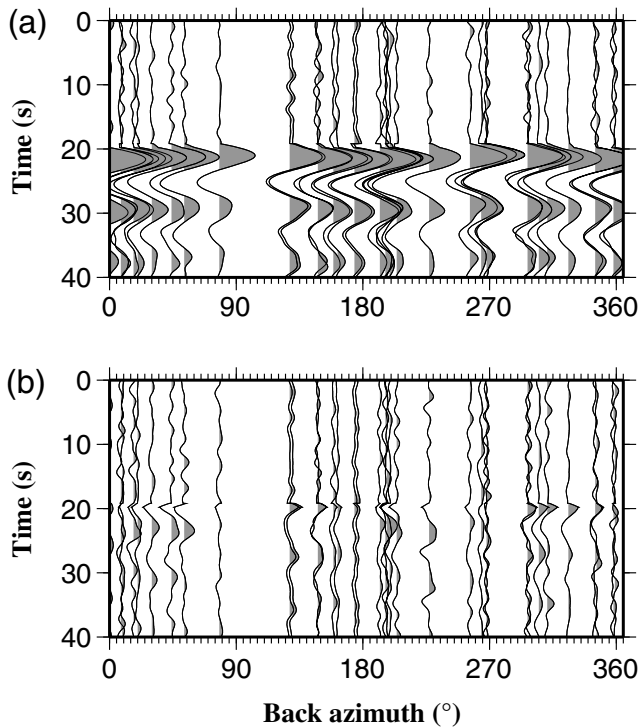


**Figure 1.** Examples of synthetic seismograms with a signal-to-noise ratio (SNR) of 8.0 computed under a simple anisotropy model with a  $\phi$  of  $90^\circ$  and a  $\delta t$  of 0.6 s. The back azimuth (BAZ) of the events is randomly selected. (a) Original radial components plotted against BAZ. (b) Original transverse components plotted against BAZ.

and slow components. After traveling through the upper layer, the two pairs of fast and slow waves are summed in the time domain and rotated to the radial and transverse directions to produce the synthetic seismograms using the same procedure as that used for the one-layer model.

#### Measuring Techniques

The splitting parameters based on TM are calculated using the procedure of Liu and Gao (2013) for making SWS measurements. The procedure initially sets the XKS window as 5 s before and 20 s after the predicted XKS arrival calculated using the IASP91 Earth model. It applies a band-pass filter in the 0.04–0.5 Hz initial range to the original radial and transverse components to enhance the SNR, and automatically rejects events with an SNR lower than 3.0 on the radial component. The resulting SWS measurements are automatically ranked into four groups: A (excellent), B (good), C (bad), and N (null) based on the SNR on the original radial, original transverse, and corrected transverse components (Liu *et al.*, 2008; Liu and Gao, 2013). Only quality A and B measurements are kept. The last step of the procedure is to manually screen the waveforms to verify and adjust (if necessary) the beginning and end times of the XKS window, the band-pass filtering parameters, and the ranking results. In this study, manual screening is applied to real data, but not to synthetic data, for the following reasons:

1. The main purpose for manual screening is to adjust the XKS window to exclude non-XKS arrivals. Such arrivals are absent in the synthetic data.
2. The frequency composition of the synthetic XKS waveform is known, thus adjusting the filtering parameters is not necessary. The corresponding standard deviation ( $\sigma$ ) for the parameters (simple  $\sigma$  for  $\delta t$  and circular  $\sigma$  for  $\phi$ ) is computed based on the resulting individual measurements. For complex anisotropy models, which are characterized by systematic azimuthal variations of the splitting parameters, the resulting parameters are displayed against the BAZ.

To measure splitting parameters based on SI, we use the same band-pass filtering criteria to preprocess the data and apply a Wiener filter to standardize the waveforms from all events. We use the suggested value of 0.001 for the water level when applying the Wiener filter (Monteiller and Chevrot, 2010) and define the signal time window the same as that for TM. The calculated splitting intensities are then stacked into  $10^\circ$  BAZ bins to enhance the reliability of measurements. The splitting parameters are found by fitting the azimuthal variation of the splitting intensities using a sine function. The amplitude of the fitting function is related to the splitting time, and the phase shift is associated with the fast orientation (Chevrot, 2000). We apply a bootstrap method to calculate the splitting parameters 10 times (Efron and Tibshirani, 1986; Press *et al.*, 1992) to estimate the  $\sigma$  of the resulting  $\phi$  and  $\delta t$  from SI.

#### Noise Resistance

We construct a simple anisotropy model with a  $\phi$  of  $90^\circ$  and a  $\delta t$  of 0.6 s to test the reliability of the resulting splitting parameters from TM and SI, using noisy synthetic data with SNR ranging from 1.0 to 10.0 with an increment of 1.0. The dominant period is set as 8.0 s. The resulting  $\phi$  and  $\delta t$  with respect to SNR (Fig. 2) show that with  $\text{SNR} \geq 3.0$ , both methods can lead to reliable results.

#### Dominant Frequency Dependence

To test the frequency dependence of the resulting parameters, we generate a set of synthetic data with different dominant periods for the presplitting radial component under a simple anisotropy model with  $\phi = 90^\circ$  and  $\delta t = 0.6$  s. The dominant period ranges from 1 to 20 s with an increment of 1 s, and the SNR is set as 10.0.

The resulting splitting parameters (Fig. 3) show that overall both TM and SI can provide reliable measurements with different dominant frequencies. The splitting parameters obtained using SI are less dependent on the dominant periods, because the Wiener filter is a shaping filter that alters the dominant frequency of the seismogram to that of the desired wavelet. The conclusion from the above tests suggests the two methods produce comparable results in the main XKS frequency bands with moderate SNR.

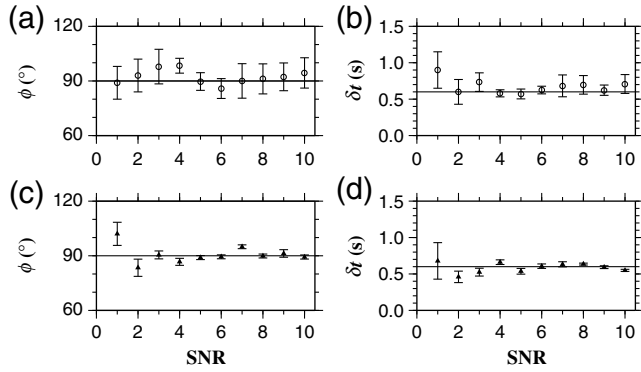


**Figure 2.** Variations of (a,c) fast orientations and (b,d) splitting times as a function of SNR. The dominant period of the seismograms is 8.0 s. (a) and (b) show results obtained using transverse minimization (TM), whereas (c) and (d) show results from splitting intensity (SI). The horizontal lines show the parameters of the simple model of anisotropy used to generate the synthetic seismograms.

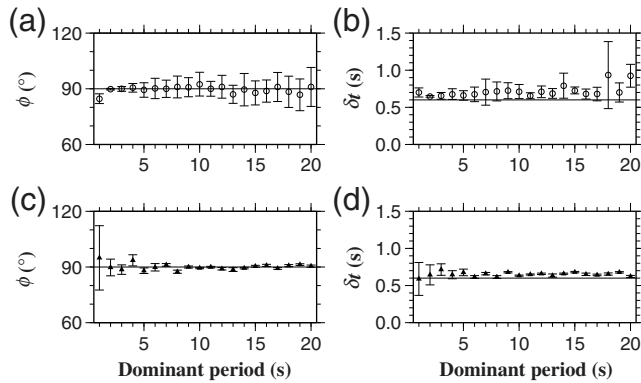


**Figure 3.** Same as Figure 2 but for the resulting splitting parameters with respect to the dominant period. The SNR is fixed at 10.0.

### Complex Anisotropy Recognition

To investigate the capability of TM and SI in complex anisotropy recognition, we construct a two-layer anisotropy model with splitting parameters of  $0^\circ$ , 0.6 s for the lower layer and  $60^\circ$ , 0.5 s for the upper layer. We generate a data set of 36 events with an SNR of 10.0 and a dominant period of 8.0 s. Figure 4a and b shows the apparent splitting parameters calculated using TM, which demonstrates a clear  $90^\circ$  periodicity over BAZ, suggesting a complex anisotropy model (Silver and Savage, 1994; Bonnin *et al.*, 2012).

The splitting intensities (Fig. 4c) computed using SI are well defined and follow a sine function well with a resulting pair of splitting parameters of  $\phi = 26.3^\circ$  and  $\delta t = 0.57$  s which are related with the splitting parameters of the two layers by  $\delta t \sin 2(\phi - \psi) = \delta t_1 \sin 2(\phi_1 - \psi) + \delta t_2 \sin 2(\phi_2 - \psi)$  (Montagner *et al.*, 2000), in which  $\phi$  and  $\delta t$  are equivalent one-layer splitting parameters,  $\psi$  is the BAZ, and  $(\phi_1, \delta t_1)$  and  $(\phi_2, \delta t_2)$  are splitting parameters of layers 1 and 2, respectively. Obviously, because SI observations from one- and two-layer anisotropy models are indistinguishably sinusoidal, if

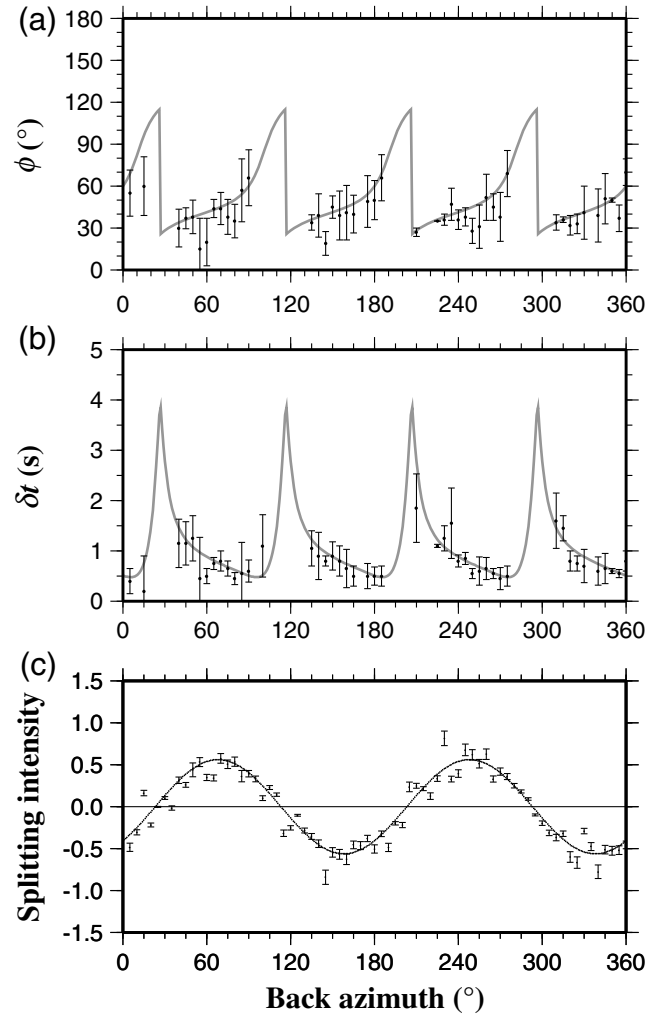


**Figure 4.** Azimuthal variations of the resulting splitting parameters measured by TM and SI under a two-layer anisotropy model: (a) fast orientations from TM, (b) splitting times from TM, and (c) splitting intensities from SI. The input parameters are  $0^\circ$ , 0.6 s for the lower layer and  $60^\circ$ , 0.5 s for the upper layer with an SNR of 10.0 and dominant period of 8 s. Solid lines in (a) and (b) are theoretical two-layer splitting parameters computed based on Silver and Savage (1994). The solid line in (c) is the best-fitting sine curve, which reveals a fast orientation of  $26.3^\circ$  and a splitting time of  $0.57$  s.

only SI is used to obtain the splitting parameters, one could incorrectly conclude the mantle beneath the station is characterized by a simple anisotropy model with a well-defined single pair of splitting parameters.

### Testing Using Real Data

We next compare the two techniques using real seismograms recorded by two broadband stations, BGCA (Bogion, Central African Republic, with a period of operation of 1994–2002) and USIN (Evansville, Indiana, 2002–2013). At USIN, no systematic azimuthal variations of the splitting parameters are revealed (Liu and Gao, 2013). On the other hand, the anisotropy structure beneath BGCA is controversial

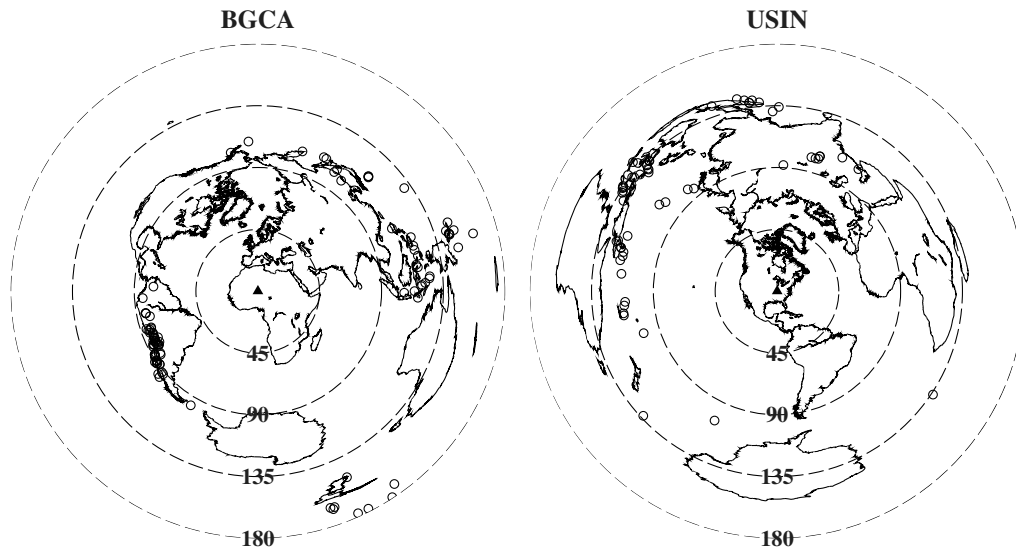


**Figure 5.** Azimuthal equidistant projection maps showing earthquakes (open dots) used in the study for (left) station BGCA and (right) station USIN. The dashed circles are centered at the stations and represent the epicentral distances in degrees.

between results obtained using various methods (Niu and Perez, 2004; Monteiller and Chevrot, 2010). The XKS data were requested from the Incorporated Research Institutions for Seismology Data Management Center for events with an epicentral distance of  $84^{\circ}$ – $180^{\circ}$  for SKS,  $90^{\circ}$ – $180^{\circ}$  for SKKS, and  $120^{\circ}$ – $180^{\circ}$  for PKS. The cutoff magnitude is 5.6 for events with a focal depth less than 100 km and 5.5 for events with a focal depth 100 km or greater to make use of sharp waveforms for all the three phases. The distribution of the teleseismic events used in the SWS analyses is shown in Figure 5, and example waveforms and Wiener-filtered traces are shown in Figures 6 and 7.

Following the procedure of Liu and Gao (2013), a total of 63 and 94 well-defined (rank A or B) measurements are obtained from USIN and BGCA, respectively. The mean fast orientation obtained at USIN is  $59.2^{\circ} \pm 7.0^{\circ}$ , and the mean splitting time is  $1.0 \pm 0.3$  s (Fig. 8), which are consistent with results from previous studies (Liu and Gao, 2013). Station-averaged results using SI are  $64.8^{\circ} \pm 5.0^{\circ}$  and  $0.77 \pm 0.1$  s (Fig. 9), which are statistically consistent with those from TM. This conclusion is consistent with that from using synthetic data.

The resulting splitting parameters using TM for station BGCA demonstrate a systematic azimuthal dependence with a period of  $90^{\circ}$  (Fig. 10), which is characteristic of a two-layer anisotropy structure (Silver and Savage, 1994). We apply a grid-search method to find the two optimal pairs of splitting parameters that can best fit the apparent splitting parameters (Silver and Savage, 1994). The resulting parameters are  $-30^{\circ}$  and 0.55 s for the lower layer and  $31^{\circ}$  and 0.9 s for the upper layer. The station-averaged splitting parameters are  $27.8^{\circ} \pm 24.0^{\circ}$  and  $0.9 \pm 0.3$  s.

By fitting the azimuthal variation of the splitting intensities using a sine function, a  $\phi$  of  $11.5^{\circ} \pm 3^{\circ}$  and a  $\delta t$  of  $0.71 \pm 0.1$  s are obtained (Fig. 11). The results are close

to the values of  $\phi = 12 \pm 2^{\circ}$  and  $\delta t = 0.65 \pm 0.1$  s reported by Monteiller and Chevrot (2010). These values are inconsistent with the station-averaged splitting parameters obtained from TM, or the parameters for the upper or lower layers. In addition, the goodness of fit of the intensities at BGCA, which is characterized by a two-layer model, is similar to that at USIN, which possesses simple anisotropy.

## Discussion and Conclusions

As discussed in Liu and Gao (2013), the XKS signal in the automatically determined (based on theoretical travel-time predictions using a 1D Earth model) XKS window can be contaminated by noise and non-XKS arrivals in both the time and spectral domains. Consequently, erroneous splitting parameters can be obtained unless careful manual screening is applied. Automatically determined results are reliable only under the ideal (and rare) condition of outstanding XKS signals on both the radial and transverse components. Such a condition requires strong XKS signals on the radial component, large splitting times, sharp waveforms, a significant deviation between the fast orientation and the BAZ, and a paucity of contamination by non-XKS arrivals. Under less than ideal conditions, manual verification of the automatically determined results and careful adjustments to the data-processing parameters are necessary to make reliable measurements. The omission of this critical step in the comparative study of Monteiller and Chevrot (2010) is mostly responsible for the conclusion that TM only works well under the rare ideal conditions.

To illustrate this point, we choose 100 events recorded by USIN with the highest SNR on the radial component and apply both the TM and SI procedures to the events, without any manual screening and adjustments to the data-processing parameters. The results from TM (Fig. 12) are inconsistent from each other, even for events from the same BAZ,

USIN (37.970, -87.670), BAZ=265.965°  
EQ062192218 (-15.798,167.789), Ev-Dep=150.0 km

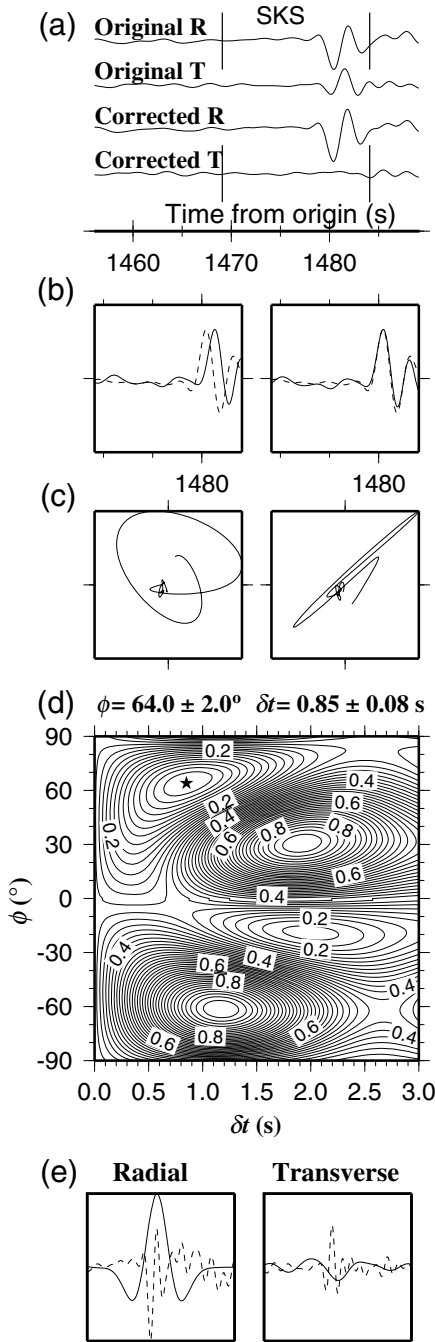


**Figure 6.** Example of shear-wave splitting measurement from an event recorded by station USIN. (a) Original radial, original transverse, corrected radial, and corrected transverse components using TM. The vertical bars define the beginning and end of the signal time window. (b) Resulting fast (dashed) and slow (solid) components (left) before and (right) after shifting the slow components in advance by the optimal splitting time. (c) Particle-motion patterns (left) before and (right) after the corrections. (d) Contour map showing the energy on the corrected transverse component with respect to fast orientation and splitting time. The star represents the optimal pair of splitting parameters that can best remove the energy on the transverse component. (e) The (left) radial and (right) transverse components before (dashed) and after (solid) Wiener filtering.

BGCA (5.180,18.420), BAZ= 231.067°  
EQ942930115 (-39.190, -70.810), Ev-Dep=161.0 km

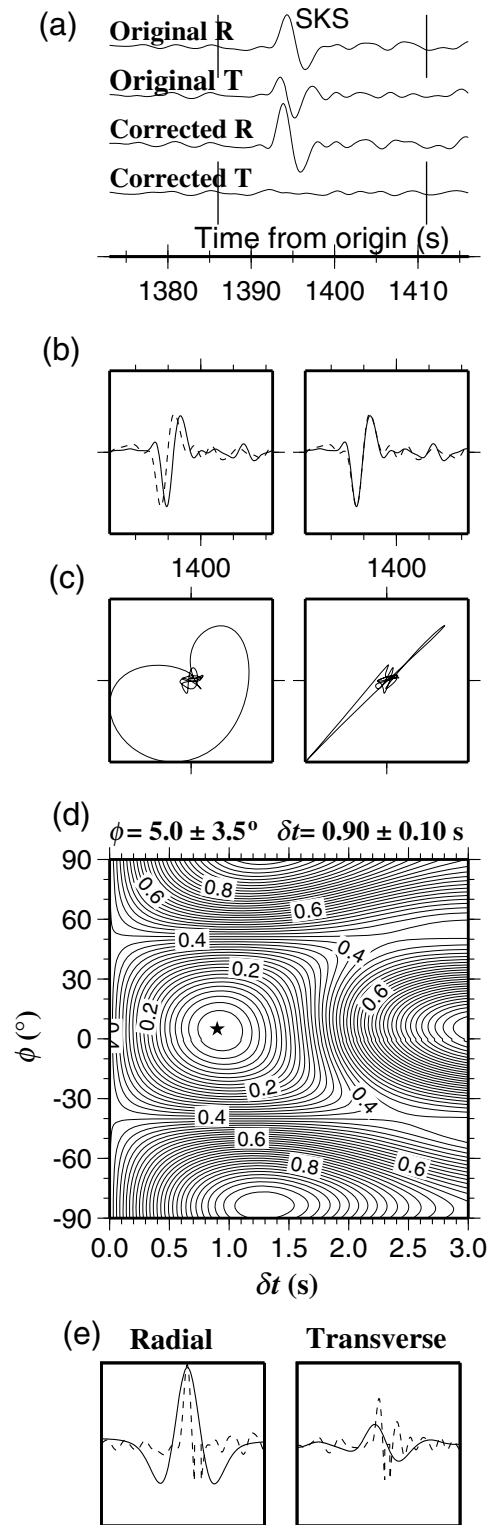


**Figure 7.** Same as Figure 6 but for an event recorded by station BGCA.

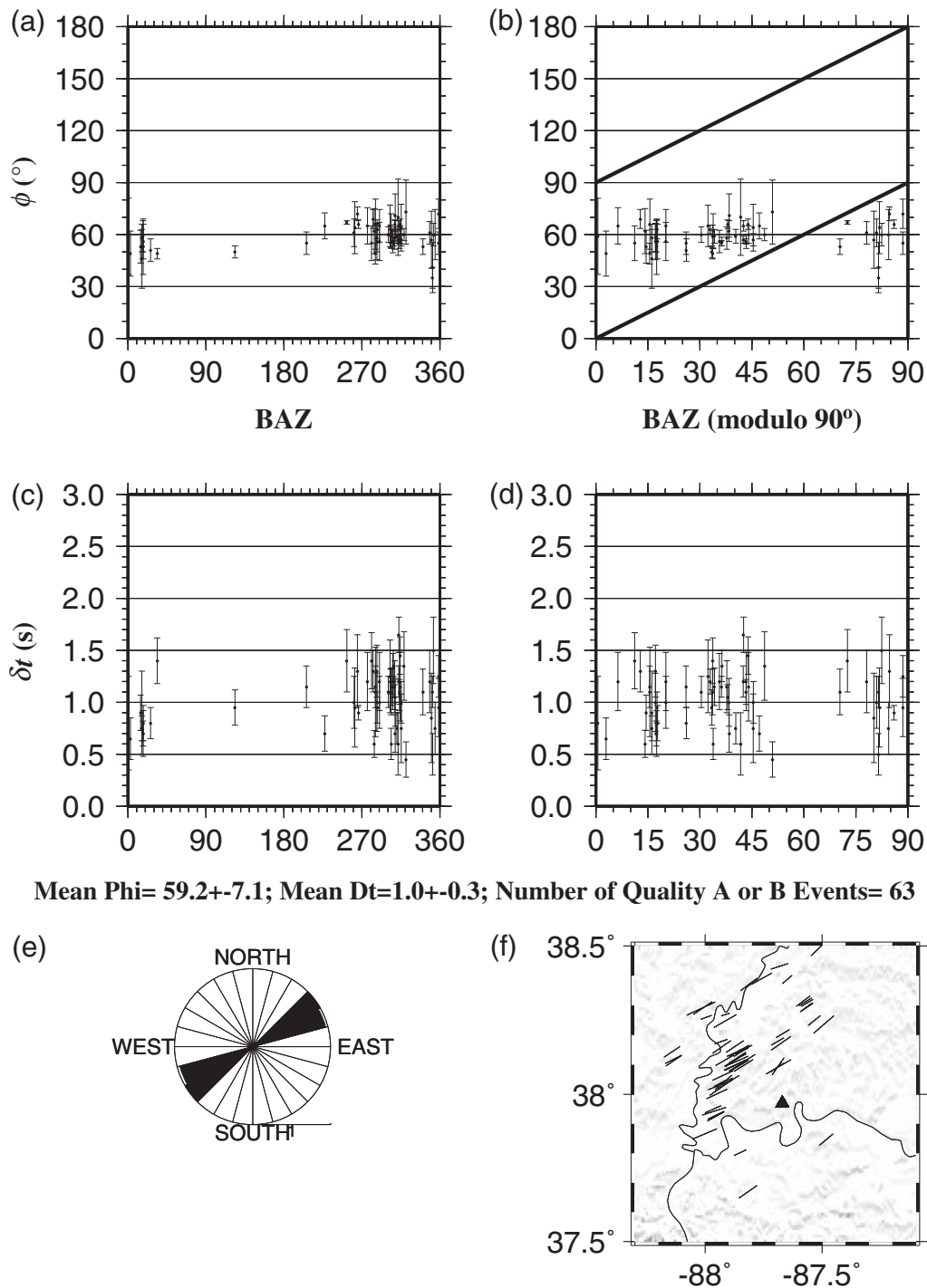


**Figure 8.** Splitting parameters observed at station USIN using TM: (a) fast orientations plotted against BAZ, (b) fast orientations plotted against modulo-90° BAZ, (c) splitting times plotted against BAZ, (d) splitting times plotted against modulo-90° BAZ, (e) rose diagram showing distribution of fast orientations, and (f) splitting parameters plotted above ray-piercing points at 200 km deep. The orientation of bars represents the fast orientation, whereas the length represents the size of the splitting time.

suggesting that many of the measurements are not reliable. Similarly, results using SI are significantly different from those obtained using manually screened waveforms (Fig. 9).

In summary, testing using both synthetic and real data demonstrates that under the simple anisotropy model, both TM and SI can obtain reliable splitting parameters, even when

the splitting times are small (e.g., 0.6 s). The testing shows the dominant frequencies of the XKS waves have insignificant effect on the resulting measurements obtained using TM or SI. However, a good azimuthal coverage is necessary for SI to obtain reliable results. In terms of detecting and characterizing complex anisotropy, TM is a powerful tool in recognizing



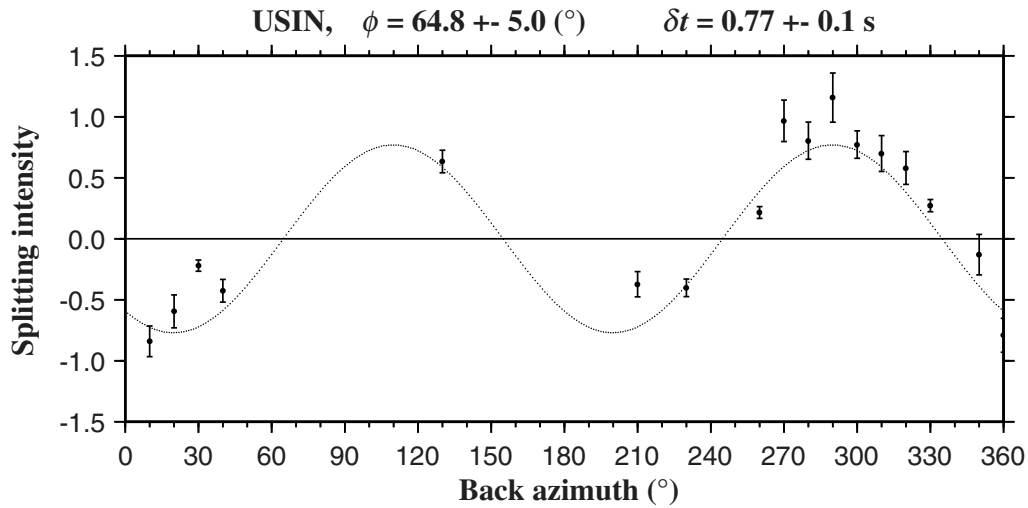


**Figure 9.** Azimuthal variations of calculated splitting intensities at station USIN after manual checking, which includes adjustments for the water level and signal time window so as to output desired wavelets (Ricker wavelet), and stacking intensities into  $10^\circ$  azimuthal window bins.

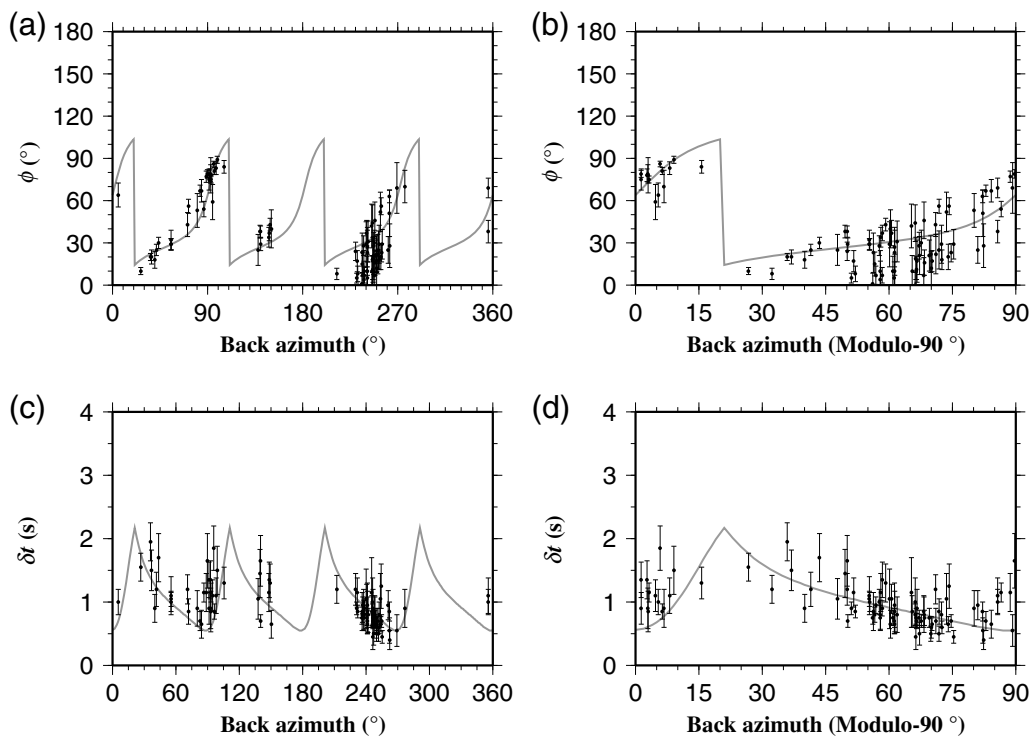


**Figure 10.** Azimuthal variations of observed-splitting parameters at station BGCA. Solid lines are the theoretical splitting parameters computed using a uniform frequency of 0.23 Hz and the two-layer parameters for this station.

complex anisotropy, which is characterized by systematic azimuthal variations of the splitting parameters. Thus when the existence of complex anisotropy beneath a station is unknown, TM is a better choice than SI for measuring SWS parameters, although for some applications such as anisotropy tomography, the latter is a more suitable choice.

#### Data and Resources

All the seismic data used in the study were obtained from the Incorporated Research Institutions for Seismology Data Management Center (<http://www.iris.edu/data/>; last accessed May 2013). The data set is publicly accessible.

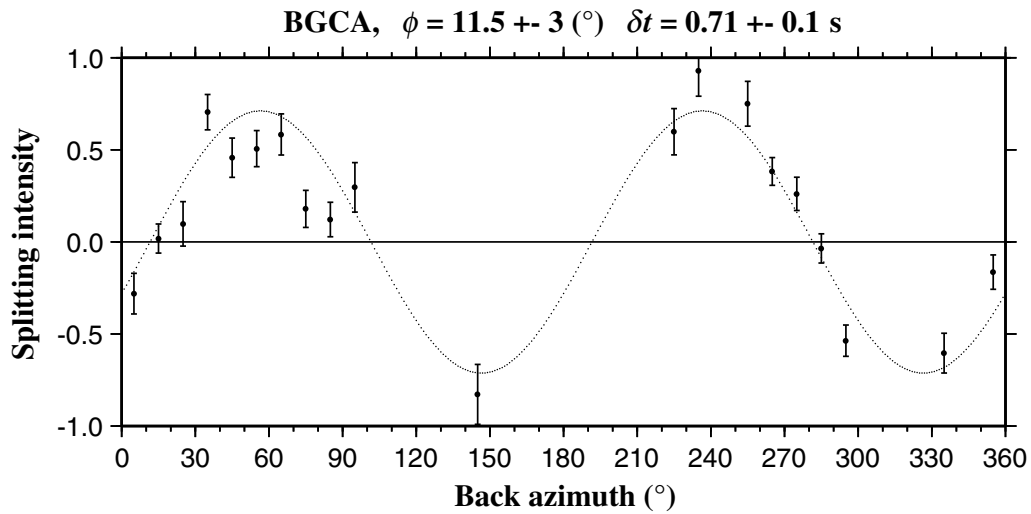


**Figure 11.** Same as Figure 9 but for station BGCA.

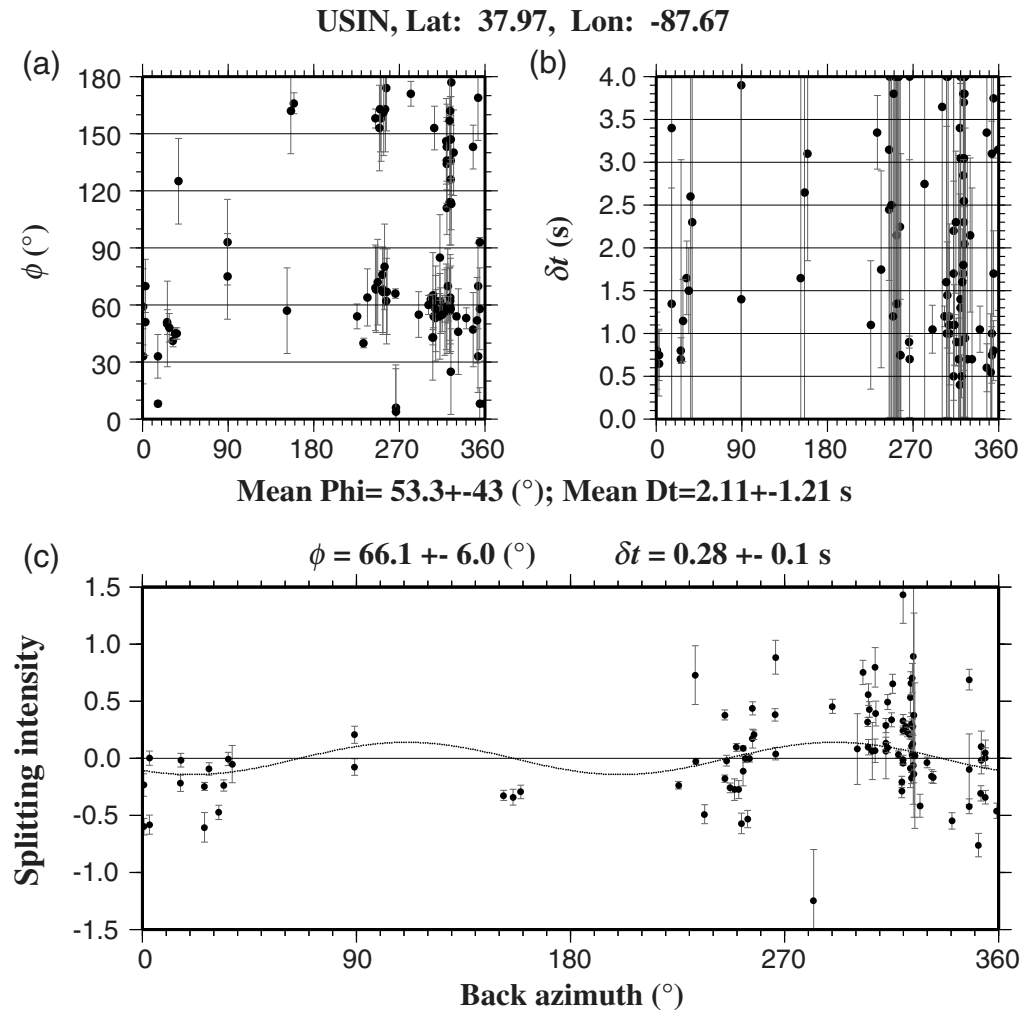


**Figure 12.** Results without manual screening obtained using 100 events with the highest SNR on the original radial component recorded by station USIN. (a) Fast orientations using TM, (b) splitting times using TM, and (c) splitting intensities using SI. The scatter in these results demonstrates the importance of manually screening the data.

## Acknowledgments

We thank S. Chevrot for assistance in the implementation of the Wiener filter, and three anonymous reviewers and Associate Editor Eric Chael for constructive suggestions. This study was partially supported by the U.S. National Science Foundation under Grant EAR-1009946 and Statoil.

## References

- Bonnin, M., A. Tommasi, R. Hassani, S. Chevrot, J. Wookey, and G. Barruol (2012). Numerical modeling of the upper-mantle anisotropy beneath a migrating strike-slip plate boundary: The San Andreas fault system, *Geophys. J. Int.* **191**, no. 2, 436–458, doi: [10.1111/j.1365-246X.2012.05650.x](https://doi.org/10.1111/j.1365-246X.2012.05650.x).
- Bowman, J. R., and M. Ando (1987). Shear-wave splitting in the upper mantle wedge above the Tonga subduction zone, *Geophys. J. Int.* **88**, no. 1, 25–41, doi: [10.1111/j.1365-246X.1987.tb01367.x](https://doi.org/10.1111/j.1365-246X.1987.tb01367.x).
- Chevrot, S. (2000). Multichannel analysis of shear wave splitting, *J. Geophys. Res.* **105**, no. B9, 21,579–21,590, doi: [10.1029/2000JB900199](https://doi.org/10.1029/2000JB900199).
- Chevrot, S., and R. D. van der Hilst (2003). On the effects of a dipping axis of symmetry on shear wave splitting measurements in a transversely isotropic medium, *Geophys. J. Int.* **152**, no. 2, 497–505, doi: [10.1046/j.1365-246X.2003.01865.x](https://doi.org/10.1046/j.1365-246X.2003.01865.x).
- Efron, B., and R. Tibshirani (1986). Bootstrap methods for standard errors, confidence intervals, and other measures of statistical accuracy, *Stat. Sci.* **1**, no. 1, 54–75.
- Gao, S., P. M. Davis, H. Liu, P. D. Slack, Y. A. Zorin, V. V. Mordvinova, V. M. Kozhevnikov, and R. P. Meyer (1994). Seismic anisotropy and mantle flow beneath the Baikal rift zone, *Nature* **371**, no. 6493, 149–151, doi: [10.1038/371149a0](https://doi.org/10.1038/371149a0).
- Gao, S. S., K. H. Liu, and M. G. Abdelsalam (2010). Seismic anisotropy beneath the Afar depression and adjacent areas: Implications for mantle flow, *J. Geophys. Res.* **115**, no. B12, B12330, doi: [10.1029/2009JB007141](https://doi.org/10.1029/2009JB007141).
- Liu, K. H., and S. S. Gao (2013). Making reliable shear-wave splitting measurements, *Bull. Seismol. Soc. Am.* **103**, no. 5, 2680–2693, doi: [10.1785/0120120355](https://doi.org/10.1785/0120120355).
- Liu, K. H., A. Elsheikh, A. Lemnifi, U. Purevsuren, M. Ray, H. Refayee, B. B. Yang, Y. Yu, and S. S. Gao (2014). A uniform database of teleseismic shear wave splitting measurements for the western and central United States, *Geochem. Geophys. Geosyst.* **15**, no. 5, 2075–2085, doi: [10.1002/2014GC005267](https://doi.org/10.1002/2014GC005267).
- Liu, K. H., S. S. Gao, Y. Gao, and J. Wu (2008). Shear wave splitting and mantle flow associated with the deflected Pacific slab beneath north-east Asia, *J. Geophys. Res.* **113**, no. B1, B01305, doi: [10.1029/2007JB005178](https://doi.org/10.1029/2007JB005178).
- Long, M. D., and P. G. Silver (2009). Shear wave splitting and mantle anisotropy: Measurements, interpretations, and new directions, *Surv. Geophys.* **30**, 407–461, doi: [10.1007/s10712-009-9075-1](https://doi.org/10.1007/s10712-009-9075-1).
- Long, M. D., and R. D. van der Hilst (2006). Estimating shear-wave splitting parameters from broadband recordings in Japan: A comparison of three methods, *Bull. Seismol. Soc. Am.* **95**, no. 4, 1346–1358, doi: [10.1785/0120040107](https://doi.org/10.1785/0120040107).
- Montagner, J.-P., D.-A. Griot-Pommera, and J. Lavé (2000). How to relate body wave and surface wave anisotropy? *J. Geophys. Res.* **105**, no. B8, 19,015–19,027, doi: [10.1029/2000JB900015](https://doi.org/10.1029/2000JB900015).
- Monteiller, V., and S. Chevrot (2010). How to make robust splitting measurements for single-station analysis and three-dimensional imaging of seismic anisotropy, *Geophys. J. Int.* **182**, no. 1, 311–328, doi: [10.1111/j.1365-246X.2010.04608.x](https://doi.org/10.1111/j.1365-246X.2010.04608.x).
- Monteiller, V., and S. Chevrot (2011). High-resolution imaging of the deep anisotropic structure of the San Andreas fault system beneath southern California, *Geophys. J. Int.* **186**, no. 2, 418–446, doi: [10.1111/j.1365-246X.2011.05082.x](https://doi.org/10.1111/j.1365-246X.2011.05082.x).
- Niu, F., and A. M. Perez (2004). Seismic anisotropy in the lower mantle: A comparison of waveform splitting of SKS and SKKS, *Geophys. Res. Lett.* **31**, no. 24, L24612, doi: [10.1029/2004GL021196](https://doi.org/10.1029/2004GL021196).
- Press, W. H., S. A. Teukolsky, W. T. Vetterling, and B. P. Flannery (1992). *Numerical Recipes in FORTRAN*, Second Ed., Cambridge University Press, Cambridge, Massachusetts, 294 pp.
- Romanowicz, B., and H. Yuan (2012). On the interpretation of SKS splitting measurements in the presence of several layers of anisotropy, *Geophys. J. Int.* **188**, no. 3, 1129–1140, doi: [10.1111/j.1365-246X.2011.05301.x](https://doi.org/10.1111/j.1365-246X.2011.05301.x).
- Savage, M. K. (1999). Seismic anisotropy and mantle deformation: What have we learned from shear wave splitting? *Rev. Geophys.* **37**, 65–106.
- Silver, P. G., and W. W. Chan (1991). Shear wave splitting and subcontinental mantle deformation, *J. Geophys. Res.* **96**, no. B10, 16,429–16,454.
- Silver, P. G., and M. Savage (1994). The interpretation of shear-wave splitting parameters in the presence of two anisotropic layers, *Geophys. J. Int.* **119**, no. 3, 949–963, doi: [10.1111/j.1365-246X.1994.tb04027.x](https://doi.org/10.1111/j.1365-246X.1994.tb04027.x).
- Vecsey, L., J. Plomerová, and V. Babuška (2008). Shear-wave splitting measurements—Problems and solutions, *Tectonophysics* **462**, nos. 1/4, 178–196, doi: [10.1016/j.tecto.2008.01.021](https://doi.org/10.1016/j.tecto.2008.01.021).
- Yang, B. B., S. S. Gao, K. H. Liu, A. A. Elsheikh, A. A. Lemnifi, H. A. Refayee, and Y. Yu (2014). Seismic anisotropy and mantle flow beneath the northern Great Plains of North America, *J. Geophys. Res.* **119**, 1971–1985, doi: [10.1002/2013JB010561](https://doi.org/10.1002/2013JB010561).

Geology and Geophysics Program  
Missouri University of Science and Technology  
Rolla, Missouri 65409  
fk36@mst.edu  
sgao@mst.edu  
liukh@mst.edu

Manuscript received 16 April 2014;  
Published Online 9 December 2014